THE JOURNAL OF BIOLOGICAL CHEMISTRY
Vol. 276, No. 25, Issue of June 22, pp. 22756–22763, 2001

Printed in U.S.A.

Allergic Cross-reactivity Made Visible

SOLUTION STRUCTURE OF THE MAJOR CHERRY ALLERGEN Pru av 1*

Received for publication, February 22, 2001, and in revised form, April 2, 2001
Published, JBC Papers in Press, April 3, 2001, DOI 10.1074/jbc.M101657200

Philipp Neudecker‡§, Kristian Schweimer‡, Jörg Nerkamp‡, Stephan Scheurer¶, Stefan Vieths¶, Heinrich Sticht‡, and Paul Rösch‡‖

From the ‡Lehrstuhl für Biopolymere, Universität Bayreuth, D-95440 Bayreuth, Germany and the ¶Abteilung Allergologie, Paul-Ehrlich-Institut, Paul-Ehrlich-Straβe 51–59, D-63225 Langen, Germany

Birch pollinosis is often accompanied by hypersensitivity to fruit as a consequence of the cross-reaction of pollen allergen-specific IgE antibodies with homologous food proteins. To provide a basis for examining the cross-reactivity on a structural level, we used heteronuclear multidimensional NMR spectroscopy to determine the high-resolution three-dimensional structure of the major cherry allergen, Pru av 1, in solution. Based on a detailed comparison of the virtually identical structures of Pru av 1 and Bet v 1, the major birch pollen allergen, we propose an explanation for a significant aspect of the observed cross-reactivity pattern among the family of allergens under consideration. The large hydrophobic cavity expected to be important for the still unknown physiological function of Bet v 1 is conserved in Pru av 1. Structural homology to a domain of human MLN64 associated with cholesterol transport suggests phytosteroids as putative ligands for Pru av 1. NMR spectroscopy provides experimental evidence that Pru av 1 interacts with phytosteroids, and molecular modeling shows that the hydrophobic cavity is large enough to accommodate two such molecules.

Birch pollinosis is one of the prevailing allergic diseases in regions with birch trees, such as Northern and Central Europe and Northern America. Up to 70% of birch pollen allergic patients who suffer from clinical syndromes like hay fever and asthma also show hypersensitivity to fresh fruit or vegetables (1). The allergic reactions after ingestion of foodstuff are predominantly oropharyngeal, for example itching and swelling of the lips, tongue, and throat, but in rare cases even severe anaphylactic reactions are possible. The symptoms of these type I allergies are caused by an immune response that is triggered when two receptor-bound IgE antibodies on the surface of a mast cell or basophil are cross-linked by simultaneous binding of an otherwise harmless antigen, the so-called allergen (2). Pollen-associated food allergies are a consequence of the cross-reaction of pollen allergen-specific IgE antibodies with highly homologous proteins contained in foodstuff. The 17.4-kDa major birch (*Betula verrucosa*) pollen allergen, Bet v 1, is responsible for IgE binding in more than 95% of birch pollen allergic patients (3). A series of allergens with high sequence identity to Bet v 1 have been reported in the literature, pollen allergens from other trees belonging to the *Fagales* order as well as food allergens like, for example, Api g 1 from celery (*Apium graveolens* (4)), Mal d 1 from apple (*Malus domestica* (5)), Pru av 1 (formerly Pru a 1) from cherry (*Prunus avium* (6)), Pyr c 1 from pear (*Pyrus communis* (7)), and Cor a 1.0401 from hazelnut (*Corylus avellana* (8)) (Fig. 1). In contrast to the three-dimensional structure of Bet v 1, which has been studied extensively in recent years (9–12), as yet no high-resolution structure of any of the corresponding food allergens is available. Because this is a prerequisite for a detailed understanding of the observed immune cross-reactivity on a structural level, we determined the three-dimensional structure of the major cherry allergen Pru av 1 in solution. Like Bet v 1, Pru av 1 is produced as a 160-residue precursor protein that is processed by cleavage of the NH_2-terminal methionine (13), yielding a protein with a calculated molecular mass of 17.5-kDa and a calculated isoelectric point of 5.9. The physiological function of these allergens is still unknown. They show high sequence similarity to pathogenesis-related and stress-induced proteins (14, 15) but seem to be expressed constitutively, even though the expression of several genes related to Bet v 1 has been reported to be induced upon contact with microorganisms (16). A potential ribonuclease activity of Bet v 1 was also discussed (17). Three highly conserved regions on the surface of the Bet v 1 molecule were proposed as candidates for IgE antibody binding epitopes (10); one of them, the glycine-rich P-loop around Glu^{45}, was recently confirmed by the crystal structure of Bet v 1 in complex with an Fab fragment of a monoclonal murine IgG antibody with high capacity to inhibit binding of serum IgE from allergic patients to Bet v 1 (18). Additional information on potential epitopes is provided by biochemical data like the study of low IgE-binding isoforms or mutants for both Bet v 1 (12, 19) and Pru av 1 (20). A thorough knowledge of the IgE binding epitopes is the key to the development of hypoallergenic allergen variants that can be used as vaccines for a patient-tailored specific immunotherapy with reduced anaphylactic side effects (21).

* This work was supported by grants from the Deutsche Forschungsgemeinschaft (Ro617/11-1) and the Bundesministerium für Bildung und Forschung (BMBF). The costs of publication of this article were defrayed in part by the payment of page charges. This article must therefore be hereby marked "*advertisement*" in accordance with 18 U.S.C. Section 1734 solely to indicate this fact.

The atomic coordinates and structure factors (code 1E09) have been deposited in the Protein Data Bank, Research Collaboratory for Structural Bioinformatics, Rutgers University, New Brunswick, NJ (http://www.rcsb.org/).

§ Recipient of fellowships from the Freistaat Bayern and the Fonds des Verbandes der Chemischen Industrie in cooperation with the BMBF.

‖ To whom correspondence should be addressed: Lehrstuhl für Biopolymere, Universität Bayreuth, Universitätsstraβe 30, D-95447 Bayreuth, Germany. Tel.: +49-921-553540; Fax: +49-921-553544; E-mail: paul.roesch@uni-bayreuth.de.

MATERIALS AND METHODS

NMR Sample Preparation—We employed two different strategies to purify recombinant Pru av 1 from *Escherichia coli* lysates. The samples used for the structure determination were prepared as described previously (22, 23). For the samples used to measure $\{^1H\}^{15}N$ nuclear

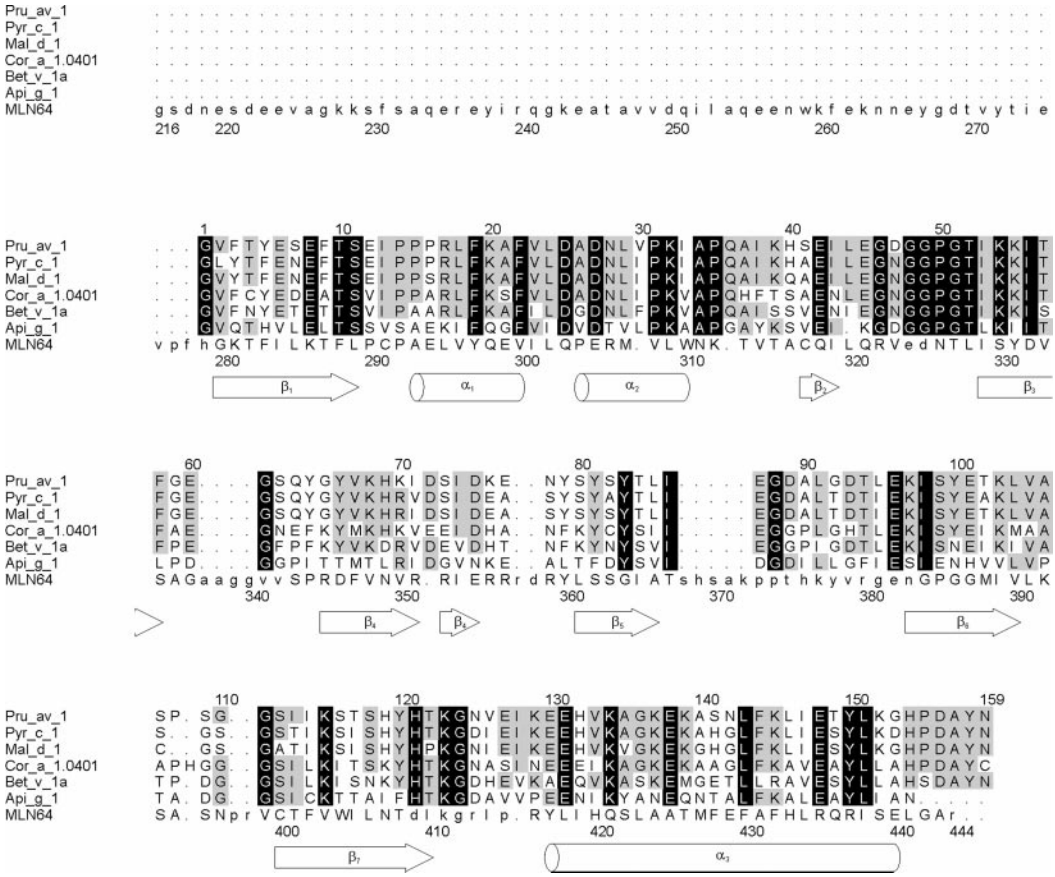

FIG. 1. **Structure-based sequence alignment with Pru av 1 of Pyr c 1 (83.5% sequence identity to Pru av 1), Mal d 1 (82.9%), Cor a 1.0401 (64.4%), Bet v 1 isoform a (59.1%), Api g 1 (41.2%), and the START domain of MLN64 (8.5%).** The sequence positions above and below the sequences correspond to Pru av 1 and MLN64, respectively. Gaps in the alignment are indicated by *dots*. Residues conserved in at least four of the six allergens are *highlighted* by *gray boxes* and residues conserved in all six allergens by *black boxes*. The secondary structure elements of Pru av 1 are shown below the alignment. The alignment of the allergens with Pru av 1 is based on homology models created by SWISS-MODEL (55) using the lowest energy structure of Pru av 1 as a template. The alignment of the START domain of MLN64 with Pru av 1 is based on a comparison of the PDB entry of the START domain of MLN64 with the lowest energy structure of Pru av 1 by the Dali server (53). The 129 MLN64 residues used for the alignment are printed in *uppercase letters* and residues not used for the alignment in *lowercase*. Formatting was performed using ALSCRIPT (56).

Overhauser effect (NOE)[1] values and to investigate the interaction with homocastasterone, a completely native purification protocol of non-fusion Pru av 1 based on chromatofocusing (24) was carried out. Final purification was achieved by anion exchange chromatography. The NMR spectra of the uniformly ^{15}N-labeled sample used for these measurements were virtually identical to those of the samples used for the structure determination except for minor changes for the NH_2-terminal residues up to Phe^3 and the loop from Thr^{122} to Lys^{129}, which is located next to the NH_2 terminus in the three-dimensional structure. Part of the sample retained the NH_2-terminal methionine in the course of the native purification protocol as verified by NH_2-terminal sequencing and observed in the NMR spectra. Homocastasterone was purchased from CIDtech Research Inc., Cambridge, Ontario, Canada, Me_2SO-d_6 from euriso-top, Gif-sur-Yvette, France. The NMR samples contained 0.8–1.2 mM uniformly ^{15}N- or $^{13}C/^{15}N$-labeled Pru av 1 and 10 mM potassium phosphate (pH 7.0) in H_2O/D_2O (9:1) or H_2O/Me_2SO-d_6 (9:1).

NMR Spectroscopy—All NMR spectra were recorded on a Bruker DRX 600 NMR spectrometer with pulsed field gradient capabilities at a temperature of either 25 or 35 °C. In addition to the experiments described previously (23) the following experiments were conducted to collect NOESY data: three-dimensional ^{15}N NOESYHSQC (120-ms mixing time (25)), ^{13}C NOESYHSQC (120-ms mixing time (26)), ^{15}N HMQCNOESYHSQC (150-ms mixing time (27, 28)), $^{13}C,^{15}N$ HMQC-NOESYHSQC (120-ms mixing time (29)), and ^{15}N-filtered two-dimensional $[^1H,^1H]$ NOESY (120-ms mixing time (23)). In the amide-detected experiments a binomial 3–9-19 WATERGATE sequence (30) with water flip-back and in the ^{13}C-edited NOESY experiments gradient coherence selection (31) was employed for water suppression. Quadrature detection in the indirect dimensions was achieved by the States-TPPI (time-proportional phase incrementation) method (32). Slowly exchanging amide protons were identified from a $[^1H,^{15}N]$ HSQC recorded after the sample had been dialyzed against 10 mM potassium phosphate (pH 7.0) in D_2O for 4 h. $\{^1H\}^{15}N$ NOE values were measured using the pulse sequence of Dayie and Wagner (33) with a relaxation delay of 4 s. For proton saturation a train of 120° high-power pulses was applied for the final 3 s of the relaxation delay. The NMR data were processed using software written in-house and analyzed with the program packages NMRView (34) and NDEE (SpinUp Inc., Dortmund, Germany). $\{^1H\}^{15}N$ NOEs were corrected for signal decrease because of minor sample precipitation during the experiment and averaged over two independent data sets.

Structure Calculation—Based on the almost complete assignment of the ^1H, ^{13}C, and ^{15}N resonances of Pru av 1 published previously (23), a total of 2299 distance restraints could be derived from the two- and three-dimensional NOESY spectra in an iterative procedure. NOE cross-peaks were classified manually as strong, medium, or weak according to their intensities and converted into distance restraints of less than 2.7, 3.5, or 5.0 Å, respectively. 23 of the 97 $^3J_{HNH_\alpha}$ scalar coupling constants measured (23) were smaller than 6.0 Hz, indicating Φ backbone torsion angles between −80° and −40°. For the 48 $^3J_{HNH_\alpha}$ coupling constants greater than 8.0 Hz, the corresponding Φ angles were restrained to between −160° and −80°. A hydrogen bond was assumed if the acceptor of a slowly exchanging amide proton could be identified unambiguously from the results of initial structure calculations. For each of the 34 hydrogen bonds the distance between the amide proton and the acceptor was restrained to less than 2.3 Å and the distance between the amide nitrogen and the acceptor to less than 3.3 Å. These experimental restraints served as an input for the calculation of 60

[1] The abbreviations used are: NOE, nuclear Overhauser effect; NOESY, nuclear Overhauser effect spectroscopy; r.m.s.d., root mean square deviation(s).

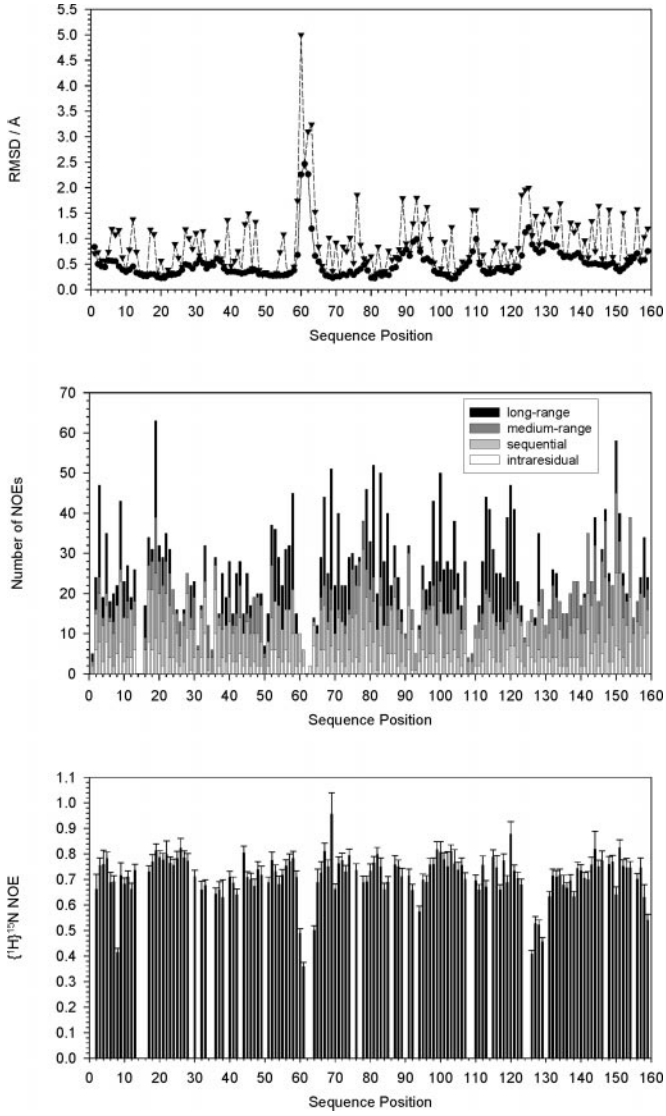

FIG. 2. **Atomic r.m.s.d. from the average structure (*top*), distribution of NOEs (*center*), and {^{1}H}^{15}N NOE values (*bottom*).** Backbone r.m.s.d. are indicated by *filled circles* and side-chain heavy atom r.m.s.d. by *filled triangles*. *Error bars* for the {^{1}H}^{15}N NOEs are shown on top of each {^{1}H}^{15}N NOE *bar*. The low number of NOE distance restraints found for the loop from Glu^{60} to Tyr^{64} leads to very high atomic r.m.s.d. As far as Pro^{14} and Pro^{15} are concerned, the lack of NOE distance restraints was compensated for by the identification of two hydrogen bonds with the slowly exchanging amide protons of Leu^{18} and Phe^{19}, respectively. The residues with a high number of NOEs are predominantly aromatic (*e.g.* Phe^{19}, Tyr^{150}, and Phe^{81}), emphasizing the importance of the ^{15}N-filtered NOESY for the structure determination. {^{1}H}^{15}N NOE values for Val^2, Phe^3, and Thr^{122} to Lys^{129} were measured for the natively purified protein.

structures using restrained molecular dynamics with X-PLOR 3.851 (35). To this end, a three-stage simulated annealing protocol (36–38) with floating assignment of prochiral groups (39) was carried out as described previously (11, 40, 41), with the following modifications. For conformational space sampling, 160 ps with a time step of 2 fs were simulated at a temperature of 2000 K, followed by 120 ps of slow cooling to 1000 K and 90 ps of cooling to 100 K, both with a time step of 1 fs. Simulation times longer than these were tested, but no significant improvement of the results could be observed. A conformational data base term for both backbone and side-chain dihedral angles (42) was included in the target function to improve the stereochemical properties of the structures. After simulated annealing the structures were subjected to 250 steps of Powell minimization (43) of the full target function followed by 1000 steps without recourse to the conformational data base potential. The 22 structures showing the lowest energy values (excluding conformational data base potential) were selected for further characterization using X-PLOR 3.851 (35) and PROCHECK 3.4 (44). Together with the experimental restraints, the atomic coordinates of this set of 22 structures have been deposited with the Protein Data Bank (PDB accession code 1E09).

Complete Cross-validation—For complete cross-validation (45) the NOE distance restraints were randomly partitioned into 10 test sets of roughly equal size (between 211 and 245). 10 sets of 60 structures were calculated, each of the sets having one of the distance restraint test sets left out. For those 16 structures of each set showing the lowest energy values, the r.m.s.d. from the distance restraints not used for their calculation were determined after assigning the restraints from the nine working sets a relative weight of 10 compared with those from the test set to prioritize them during floating assignment of prochiral groups.

Patients' Sera—Sera from patients allergic to birch pollen and with an oral allergy syndrome after ingestion of fresh fruits (cherry, apple, pear, hazelnut) and vegetables (celery) were selected for this study. Most of the sera showed positive CAP or EAST (enzyme allergo-sorbent test) classes (greater than class 2) to the major allergens of birch pollen (Bet v 1), celery (Api g 1), cherry (Pru av 1), apple (Mal d 1), and pear (Pyr c 1). Sera were taken from the serum collection of the Paul-Ehrlich-Institut or kindly supplied by Dr. H. Aulepp (Hospital Borkum Riff, Borkum, Germany).

Recombinant Allergens for Immunoblot Experiments—The recombinant major allergens from birch pollen, Bet v 1 isoform a, apple, Mal d 1, and celery tuber, Api g 1, were obtained from BIOMAY, Linz, Austria. The recombinant major allergen from sweet cherry, Pru av 1, was purified as described elsewhere (6). The major allergens from pear, Pyr c 1 (GenBank™ accession number AF057030), and from hazelnut, Cor a 1.0401 (GenBank™ accession number AF136945), were purified as non-fusion proteins and kindly supplied by Dr. F. Karamloo and D. Lüttkopf (Paul-Ehrlich-Institut, Langen, Germany).

SDS-Gel Electrophoresis, Immunoblotting, and Immunoblot Inhibition—The purified recombinant allergens were analyzed by SDS-polyacrylamide gel electrophoresis under nonreducing conditions according to Laemmli (46). IgE immunoblotting was performed by a modification of a previously described procedure (47). Briefly, for immunoblot analysis the allergens (0.5 μg/cm slot) were electrophoretically transferred onto nitrocellulose membranes (0.45 μm, Schleicher & Schuell) by tank blotting. For immunoblot inhibition 20 μl of a pooled patient serum was preincubated with 15 μg of Bet v 1a, 10 μg of Pru av 1, 10 μg of Api g 1, and buffer as control for 5 h. Thereafter, samples were diluted to 0.6 ml (1 ml for the samples with Bet v 1a as an inhibitor) and added to the blot strips (3 mm width). After overnight incubation, bound IgE was detected with a rabbit anti-human IgE antiserum (1:4000, 1 h; DAKO, Glostrup, Denmark) followed by a biotin-labeled goat anti-rabbit immunoglobulin antibody (1:6000, 1 h; DAKO) as a secondary antibody and a streptavidin-horseradish peroxidase (Amersham Pharmacia Biotech, Little Chalfont, Buckinghamshire, UK) incubation (1:10000, 30 min). Visualization was performed with the ECL™ Western blotting detection reagents (Amersham Pharmacia Biotech).

Modeling of Allergen-Steroid Complexes—Cavities were examined with SURFNET 1.5 (48) using a grid separation of 1.0 Å and a minimum and maximum gap sphere radius of 1.4 and 3.5 Å, respectively. Topology and parameter files for cholesterol were generated by the HIC-Up server (49) based on the cholesteryl linoleate moiety of a crystal structure (50) from which the linoleate atoms were removed and subsequently modified to obtain topology and parameter files for castasterone. The simulated annealing protocol described above was also used to model Bet v 1 complexes with castasterone. To this end the atom positions of Bet v 1 as given by its crystal structure (10) were kept fixed, whereas a set of 33 distance restraints between the C-8 atom of castasterone and those Cα atoms of Bet v 1 lining the cavity was introduced for each castasterone molecule, which effectively restrained C-8 to within 7.5 Å of a point near the center of the cavity. The resulting models were refined by 1000 steps of Powell minimization (43) of a modified target function where the van der Waals interaction was represented by a Lennard-Jones-type potential. The results were transferred to Pru av 1 by placing the castasterone molecules into equivalent positions of the lowest energy structure of Pru av 1, which was followed by 1000 steps of Powell minimization of the original target function (including all experimental restraints and the modeling distance restraints) to remove steric clashes and subsequent refinement by 1000 steps of Powell minimization of the modified target function (again including all restraints).

TABLE I
Summary of the structure calculation

Except for the experimental restraints, all values are average values over the 22 accepted structures in the form average value ± standard deviation.

Experimental restraints used for the structure calculation	
Intra-residual NOEs	658
Inter-residual NOEs	
Sequential	729
Medium range	330
Long range	582
Dihedral angle restraints	71
Hydrogen bonds	34
Molecular dynamics simulation statistics	
Energies/kcal/mol	
Total	244 ± 7
Bond lengths	7.1 ± 0.5
Bond angles	180 ± 3
Improper angles	22.2 ± 0.7
van der Waals repulsion	13.3 ± 1.2
Distance restraints	22 ± 3
Dihedral angle restraints	0.037 ± 0.021
r.m.s.d.s from ideal distances/Å	
Bond lengths	0.00169 ± 0.00006
Distance restraints	0.0135 ± 0.0010
r.m.s.d.s from ideal angles/°	
Bond angles	0.510 ± 0.005
Dihedral angles	0.438 ± 0.004
Dihedral angle restraints	0.028 ± 0.008

	Atomic r.m.s.d.s from the average structure	
	Backbone	Heavy atoms
	Å	
Overall[a]	0.60 ± 0.09	0.93 ± 0.09
Regular secondary structure[b]	0.41 ± 0.08	0.72 ± 0.06
β-Strands[c]	0.29 ± 0.06	0.61 ± 0.07
COOH-terminal α-helix[d]	0.39 ± 0.12	0.85 ± 0.12

Comparison with other structures		
		Å
Backbone atomic r.m.s.d.s	Bet v 1 X-ray[e]	1.94 ± 0.15
	Bet v 1 NMR[f]	2.31 ± 0.13
	MLN64	2.93 ± 0.07
	START[g]	

[a] Residues 1–159.
[b] Residues 2–58, 65–85, 97–104, 112–122, 130–153.
[c] Residues 2–11, 41–58, 65–85, 97–104, 112–122.
[d] Residues 130–153.
[e] From Ref. 10.
[f] (11); average structure; residues 1–154.
[g] (52); Residues 2–29, 31–35, 37–47, 50–60, 63–71, 73–77, 78–86, 98–110, 111–120, 129–156 (Pru av 1) with 280–307, 308–312, 313–323, 326–336, 343–351, 352–356, 359–367, 384–396, 399–408, 416–443 (MLN64), respectively.

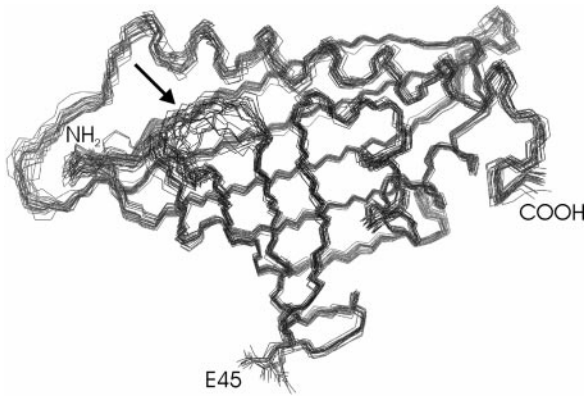

FIG. 3. **Backbone overlay of the 22 accepted structures.** The NH_2 terminus on the *left* is hidden by the loop from Ile^{86} to Glu^{96}, and the COOH terminus can be seen on the *right*. Except for the loop from Glu^{60} to Tyr^{64}, which is indicated by an *arrow*, the structures are in excellent agreement, especially as far as the β-strands are concerned. The side-chain of Glu^{45} shown at the *bottom* is clearly solvent-exposed in all structures. The overlay was performed using Sybyl 6.5 (Tripos Inc., St. Louis, MO).

RESULTS AND DISCUSSION

Structure Determination—Analysis of the NMR spectra of Pru av 1 yielded a total of 2438 experimental restraints for the structure calculation. In particular, the good dispersion of the amide proton resonances (23) allowed the identification of 1908 ^{15}N NOESYHSQC cross-peaks, thus providing the largest contribution. The ^{13}C NOESYHSQC suffered from an unsatisfactory signal-to-noise ratio because of the relatively low sample concentration, which was worsened by the presence of some degradation products in the sample. As a consequence, only 54 distance restraints were derived from this spectrum. A ^{15}N-filtered NOESY could, however, provide 337 additional distance restraints which were particularly valuable because many of them are based on long-range NOEs involving aromatic side-chains expected to form hydrophobic cores (Fig. 2). 71 dihedral angle restraints derived from $^3J_{HNH\alpha}$ scalar coupling constants and 68 distance restraints for the observed hydrogen bonds complete the set of experimental restraints used for the structure calculation (Table I). The 22 accepted structures showed no single distance restraint violation of more than 0.30 Å and no systematic violation of more than 0.15 Å. An analysis with PROCHECK 3.4 (44) revealed that 82.4% of the non-glycine and non-proline residues adopted a conformation within the most favored regions of the Ramachandran plot, and 16.6% adopted a conformation in the additional allowed regions. No residues with a conformation in the disallowed regions were observed. Even though Kuszewski and Clore (51) recently reported that the roughness of their conformational data base potential (42) as used in our calculation may affect convergence and conformational sampling in structure calculations with very few experimental restraints, no such problems occurred in the structure calculation of Pru av 1, probably because of the high number of experimental restraints. Artifacts arising from the conformational data base potential can be ruled out because a control calculation without recourse to this potential yielded an almost identical set of structures (atomic root mean square deviations (r.m.s.d.) between the two average structures were 0.65 Å for the backbone and 0.85 Å for all heavy atoms). The quality of the structure determination was also assessed by calculating a total of 600 structures for complete cross-validation (45). The value of 0.27 ± 0.07 Å for the cross-validated r.m.s.d. from the test set distance restraints of the set of 160 accepted structures indicates the high quality of the solution structure of this comparatively large protein.

Description of the Structure—Pru av 1 shows a well defined structure in solution (Fig. 3) with average atomic r.m.s.d. from the average structure of 0.60 Å for the backbone and 0.93 Å for all heavy atoms. A schematic representation of the solution structure of Pru av 1 (Fig. 4) reveals that a folded seven-stranded antiparallel β-sheet (residues 2–11, 41–43, 53–58, 65–75 with a kink at Asp^{72}, 80–85, 97–104, and 112–122) and two short α-helices arranged in a V-shaped manner (residues 15–22 and 26–33) wrap around a long COOH-terminal α-helix (residues 130–153) to form a basket-like structure with the long helix resembling a handle, thus creating a large hydrophobic cavity. In contrast to the precision of the overall structure, however, the loop from Glu^{60} to Tyr^{64} is experimentally less well defined because of the missing resonance assignments for the amide protons of Ser^{62} and Gln^{63} (23), leading to a marked increase in atomic r.m.s.d. (Fig. 2). This lack of experimental data might in fact reflect an actually existing increased

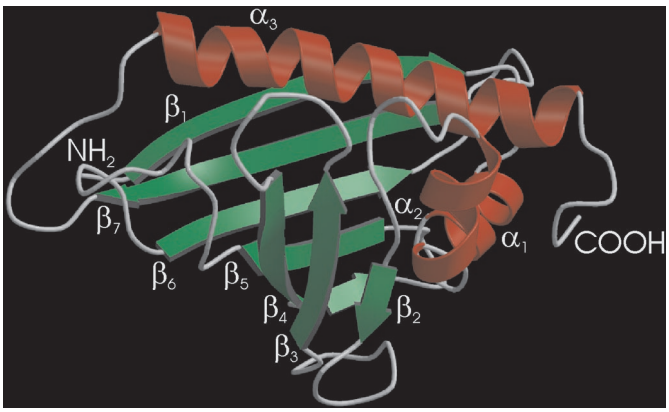

FIG. 4. **Schematic representation of the secondary structure elements based on the lowest energy structure.** The same view is shown as in Fig. 3. Despite being hidden by β_3, the kink in β_4 at Asp^{72} is clearly visible. The figure was drawn with MolScript 1.4 (57) and rendered with Raster3D 2.2a (58).

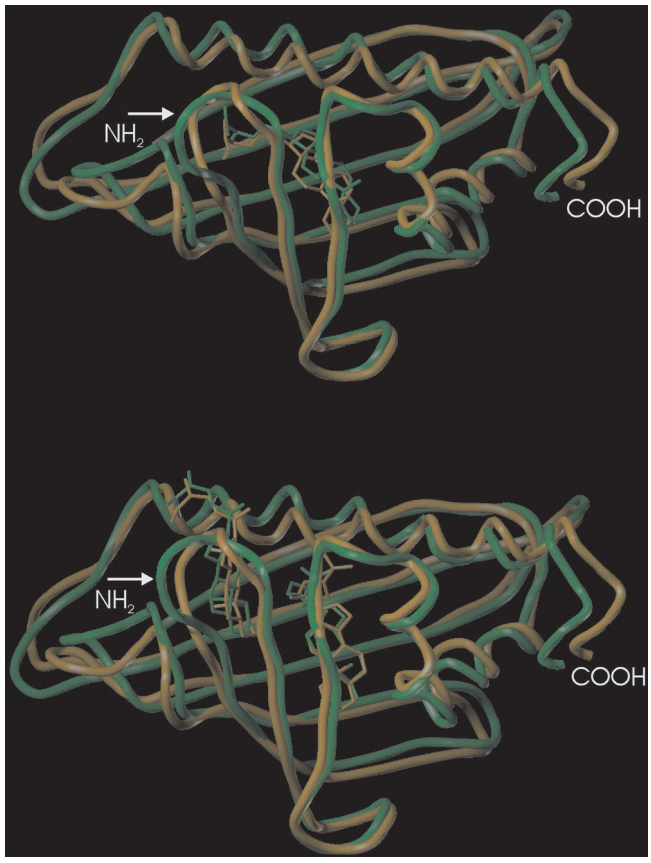

FIG. 5. **Backbone overlay of the lowest energy solution structure of Pru av 1 (*green*) and the crystal structure of Bet v 1 (*orange*) in complex with one (*top*) and two (*bottom*) castasterone molecules (representative models).** The same view is shown as in Figs. 3 and 4. The loop from Glu^{60} to Tyr^{64} is indicated by an *arrow*. The overlay was performed using Sybyl 6.5 (Tripos Inc.).

flexibility. One indication for this is the rapid solvent exchange of the amide protons in this region, resulting in exceptionally weak NMR signals. In addition, this loop is poorly defined in both sets of solution structures of Bet v 1 (10, 11), and the determination of the crystal structure of Bet v 1 yielded two conformers for this loop (*i.e.* Asp^{60} to Lys^{65}), which still do not fit the electron density well (10). To obtain initial experimental data concerning the dynamic behavior of Pru av 1 in solution we measured $\{^1H\}^{15}N$ NOE values (Fig. 2). The low $\{^1H\}^{15}N$ NOEs of 0.489 ± 0.018, 0.359 ± 0.017, and 0.501 ± 0.018 for the amide protons of Glu^{60}, Gly^{61}, and Tyr^{64}, respectively, strongly support the notion that this loop shows significantly increased internal flexibility. Surprisingly, one of the lowest values (0.414 ± 0.017) was measured for the amide proton of Glu^{8}, which is located in a slight bend in the middle of the first β-strand.

Comparison with Bet v 1—The folding topology of Pru av 1 has already been observed for the major birch pollen allergen Bet v 1, and a backbone overlay of the lowest energy structure of Pru av 1 with the crystal structure of Bet v 1 (Fig. 5; steroid molecules are modeled into these structures as discussed below) confirms that indeed both the secondary structure elements and the tertiary fold of these two allergens are virtually identical. More precisely, a comparison of the average solution structure of Pru av 1 with the crystal structure of Bet v 1 (10) and the average solution structure of Bet v 1 (Ref. 11; only residues 1–154 are taken into account, because the COOH terminus is less well defined experimentally) yields backbone atomic r.m.s.d. of 1.85 and 2.23 Å, respectively, which is of the same order as the difference of 2.06 Å found upon comparing these two Bet v 1 structures with each other. Together with the considerable sequence identity between Pru av 1 and Bet v 1, the conserved backbone conformation leads to a very similar molecular surface as far as shape and charge distribution are concerned, rendering the existence of cross-reactive IgE-binding epitopes most likely. In particular, the glycine-rich P-loop around Glu^{45} is structurally conserved in Pru av 1. For Bet v 1, this region was recently identified as the binding epitope of a monoclonal murine IgG antibody (18) whose high capacity to inhibit binding of serum IgE from allergic patients to Bet v 1 indicates that the P-loop is also one of the IgE binding epitopes. The introduction of four point mutations including the substitution of Glu^{45} by serine indeed resulted in a Bet v 1 mutant with severalfold reduced IgE binding capacity (12). In the crystal structure of the complex of Bet v 1 with the IgG Fab fragment, the negatively charged side-chain of Glu^{45} is located in a binding pocket of the antibody with a positive electrostatic potential, where it forms two hydrogen bonds. In addition to Glu^{45}, which is found to be solvent-exposed in all 22 accepted structures of Pru av 1 (Fig. 3), 14 of the remaining 15 residues forming the interaction surface between Bet v 1 and the IgG Fab fragment are either conserved (Glu^{42}, Gly^{46}, Gly^{48}, Gly^{49}, Pro^{50}, Gly^{51}, Thr^{52}, Asp^{72}, Ile^{86}, and Lys^{97}) or substituted conservatively (Ile^{44} by Leu, Asn^{47} by Asp, Arg^{70} by Lys, and His^{76} by Lys) in Pru av 1 (Fig. 1), which strongly suggests that this region is a cross-reactive IgE binding epitope. This proposal is supported by the significantly decreased binding of serum IgE to the mutants Pru av 1 G46P and Pru av 1 ΔT52 observed for some patients (20).

Immunoblot Inhibition Experiments—For IgE immunoblot inhibition experiments a serum pool of seven patients was tested with Bet v 1a, Mal d 1, Api g 1, Pru av 1, Cor a 1.0401, and Pyr c 1 transferred to nitrocellulose. Preincubation of the serum pool with Bet v 1a showed complete inhibition of IgE binding to the related major food allergens (Fig. 6). Hence, all of the IgE binding epitopes presented by these food allergens exist on the molecular surface of Bet v 1a as well. This finding is consistent with the experience that sensitization usually occurs to birch pollen, whereas the related food allergies are a consequence of the cross-reaction of the resulting pollen-specific IgE antibodies. To investigate the IgE cross-reactivity with the two major food allergens from cherry and celery, preincubation of the serum pool was performed with Pru av 1 and Api g 1. Complete inhibition of IgE binding to the major cherry allergen was obtained with Pru av 1 as the positive control. By contrast, only a small reduction of IgE binding to Pru av 1 on the solid phase resulted from using Api g 1 as an inhibitor (Fig.

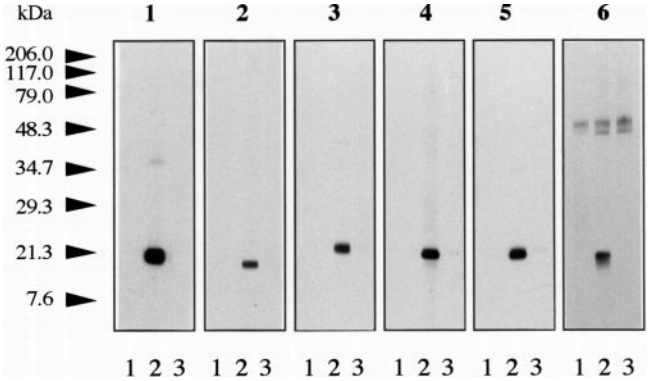

FIG. 6. **Immunoblot inhibition of IgE binding to Bet v 1a (*column 1*), Api g 1 (*column 2*), Mal d 1 (*column 3*), Pru av 1 (*column 4*), Pyr c 1 (*column 5*), and Cor a 1.0401 (*column 6*) on the solid phase.** A serum pool from birch pollinotic patients with associated food allergy was preincubated with Bet v 1a (*lanes 3*) as an inhibitor. Serum from a nonallergic subject (*lanes 1*) and samples without inhibitor (*lanes 2*) were used as controls.

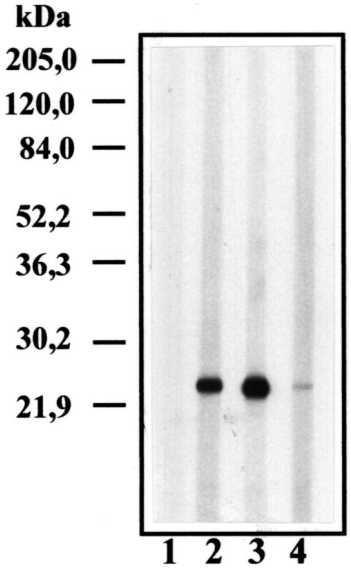

FIG. 7. **Immunoblot inhibition of IgE binding to Pru av 1 on the solid phase with Pru av 1 (*lane 1*) and Api g 1 (*lane 2*) as inhibitors.** A sample without inhibitor (*lane 3*) and serum from a nonallergic subject (*lane 4*) were used as controls.

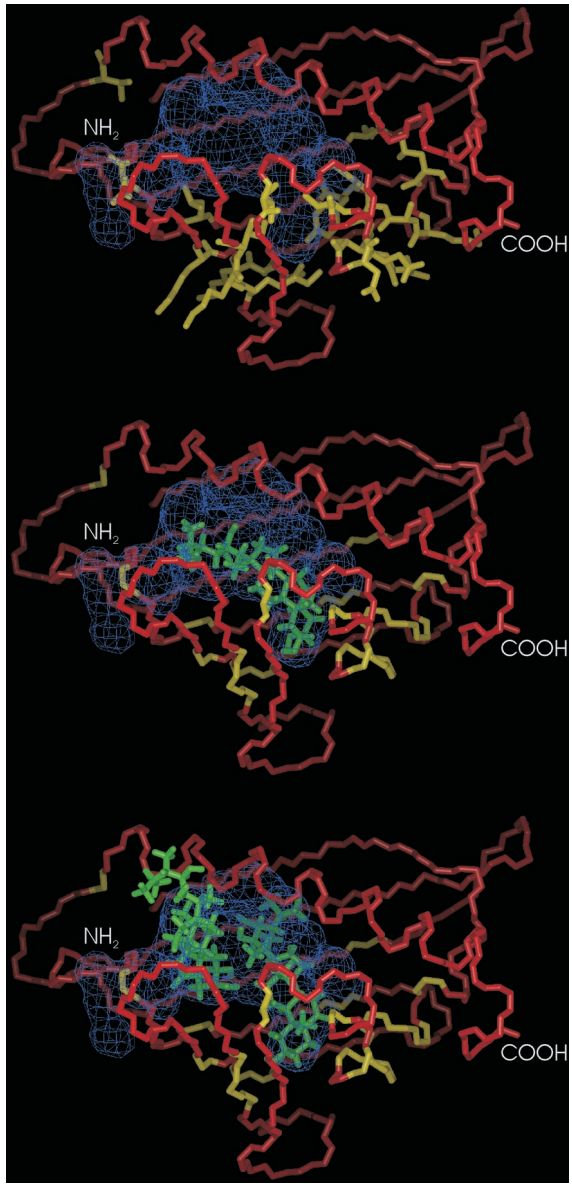

FIG. 8. **Visualization of the hydrophobic cavity.** A similar view is shown as in Figs. 3–5. A *stick* representation of the backbone heavy atoms of the lowest energy structure of Pru av 1 is shown in *red*, and the cavity is indicated by *blue lines*. Also shown are the side-chains of those residues whose amide proton resonances disappeared upon the presence of homocastasterone (*top*). These residues are colored *yellow*. The locations of one (*center*) and two (*bottom*) castasterone molecules modeled into the cavity are shown in *green*. The figure was prepared with InsightII 98.0 (Molecular Simulations Inc., San Diego).

7). No IgE inhibition was detected with buffer as control. Serum from a nonallergic donor was used as negative control. In other words, Pru av 1 must contain at least one IgE binding epitope that is not presented by Api g 1. Sequence alignment of Pru av 1 with Api g 1 (Fig. 1) shows that the P-loop region is not conserved in Api g 1; the P-loop is not only shorter by one residue, but also the negatively charged Glu^{45} is substituted by a positively charged lysine. The proposal that the P-loop region forms one of the cross-reactive epitopes can therefore provide a simple explanation of why preincubation with Api g 1 fails to efficiently inhibit IgE binding to Pru av 1. To verify this hypothesis the preparation and subsequent immunological as well as structural characterization of several allergen mutants is currently under way in our laboratories.

Implications for the Physiological Function—Bet v 1 and Pru av 1 form a large internal hydrophobic cavity with a volume of ~1600 $Å^3$ (Fig. 8). This forked cavity has three openings to the protein surface, one at the P-loop, one between α_3 and β_1, and one between α_3 and the loop from Glu^{60} to Tyr^{64}. The latter is the largest opening, but its size depends strongly on the conformation of the flexible loop acting as a flap. Such a large cavity constitutes a very unusual feature for a protein structure and can therefore be expected to be important for its physiological function. An obvious possibility for the physiological purpose of the cavity is the binding of a hydrophobic ligand. An indication of what this hypothetical ligand might be was provided by the recently determined crystal structure of the START domain of the human protein MLN64 (52), part of which revealed a striking structural homology to Bet v 1 and Pru av 1 (Fig. 9). Based on a comparison of the PDB entry of the START domain of MLN64 with the lowest energy structure of Pru av 1 by the Dali server (53), an alignment of the average solution structure of Pru av 1 with the crystal structure of the START domain of MLN64 yielded a backbone atomic r.m.s.d. of 2.89 Å over as many as 129 residues, even though the sequence identity over these 129 residues is only 8.5% (Fig. 1). Bet v 1 and the START domain of MLN64 are the only proteins with

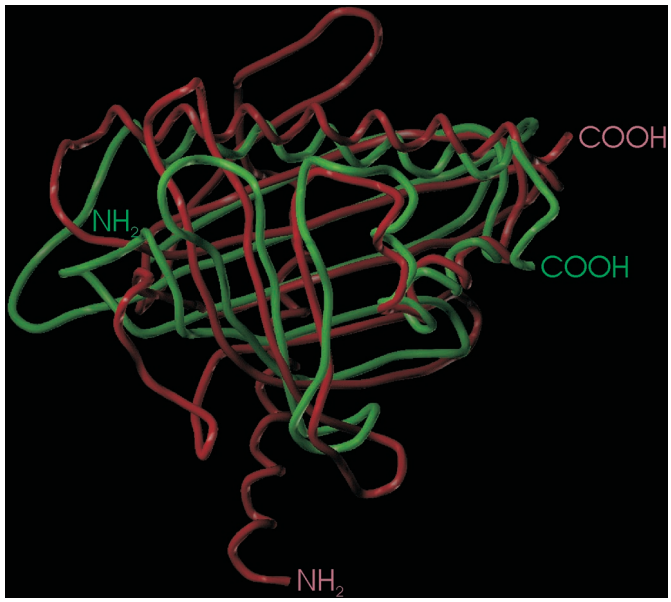

FIG. 9. **Backbone overlay of the lowest energy solution structure of Pru av 1 (*green*) and the crystal structure of the START domain of MLN64 (*red*).** The same view is shown as in Figs. 3–5. The overlay was performed using Sybyl 6.5 (Tripos Inc.).

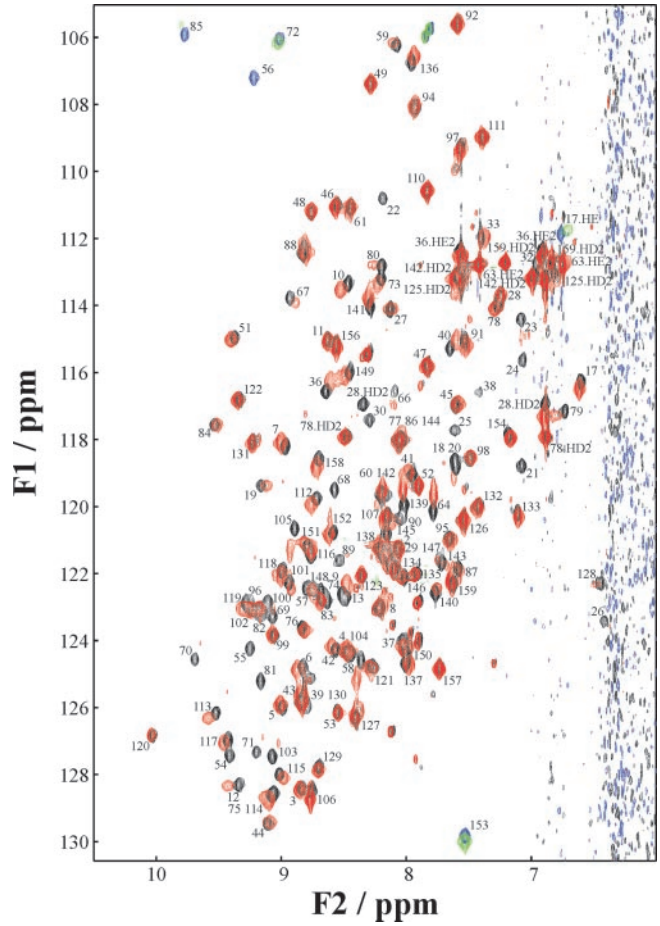

FIG. 10. **Overlay of the [^{1}H,^{15}N] HSQC spectra of uniformly ^{15}N-labeled Pru av 1 with (positive signals in *red*, negative signals in *green*) and without (positive signals in *black*, negative signals in *blue*) homocastasterone in H_2O/Me_2SO-d_6 (9:1).** Amide proton resonances are labeled according to their residue numbers. Negative resonances are aliased in the indirect ^{15}N dimension F1.

significant structural homology to the lowest energy structure of Pru av 1 that were found by a Dali server data base search. The fact that START domains are associated with the transfer of lipids, especially of steroids, suggests phytosteroids as possible ligands for Bet v 1 and Pru av 1. It should be noted, however, that there are also significant structural differences between Bet v 1 and Pru av 1 on one hand and the START domain of MLN64 on the other hand. In addition to the existence of an additional α-helix and two additional β-strands at the NH_2 terminus, the cavity of the START domain of MLN64 with a volume of about 1000 Å, which is approximately the volume required for the accommodation of a single steroid molecule, is much smaller than that of the allergens. Furthermore, the cavity of the START domain of MLN64 resembles a tunnel, with only two openings to the protein surface, which correspond to the opening at the P-loop and to the opening between α_3 and the loop from Glu60 to Tyr64 of Pru av 1. Unfortunately, a quantitative investigation of the binding of phytosteroids to Pru av 1 by means of NMR titration experiments is very difficult because of the hydrophobicity of virtually all the physiologically relevant steroids, but we were able to gather first qualitative experimental evidence that Pru av 1 does indeed interact with a particular phytosteroid. Upon the addition of homocastasterone, a brassinosteroid that is different from the most widely distributed brassinosteroid, castasterone, only by the replacement of the methyl group at C-24 with an ethyl group (54), several amide proton resonances of Pru av 1 disappeared from the [^{1}H,^{15}N] HSQC spectrum (Fig. 10). This is probably because of severe line broadening as a consequence of exchange processes that are intermediate on the NMR time scale. Interestingly, the affected residues (Leu^{18}, Lys^{20}, Ala^{21}, Phe^{22}, Val^{23}, Leu^{24}, Asp^{25}, Ala^{26}, Asn^{28}, Val^{30}, Ile^{38}, Lys^{54}, Lys^{55}, Ile^{56}, Lys^{68}, Lys^{70}, Ile^{71}, Tyr^{81}, Leu^{85}, Asp^{89}, Lys^{103}, and Ile^{128}) surround the lower part of the cavity like a funnel (Fig. 8), thus supporting the expectation that homocastasterone binding takes place inside this cavity. Molecular modeling was used to investigate the steric constraints that are imposed on the orientation and the position of bound steroid molecules by the size and shape of the cavity. Because the opening between α_3 and the loop from Glu^{60} to Tyr^{64} of the lowest energy solution structure of Pru av 1 is larger than the corresponding opening of the crystal structure of Bet v 1, we decided to model the more constrained Bet v 1 complexes first and then transfer the results to Pru av 1. The cavity of Bet v 1 and Pru av 1 is so large that it can accommodate one or two castasterone molecules in several different positions and orientations without significant structural changes (Figs. 5 and 8). In conclusion, in light of the above evidence, the physiological function of Bet v 1 and Pru av 1 most likely involves phytosteroid binding. The striking structural homology observed between the plant proteins Bet v 1 and Pru av 1 on one hand and the corresponding domain of the human protein MLN64 on the other hand, despite a low sequence identity and despite considerable structural differences, indicates that we might be dealing with a widely distributed tertiary fold designed to bind steroids or other lipids for a variety of purposes. Although our results mark a first step toward the elucidation of the physiological function of these proteins, a series of questions remains to be answered by future investigations; for example, is the binding specific for particular steroids, and if so, what features determine the specificity? Do these allergens bind two steroid molecules simultaneously, or is there any additional ligand to occupy the extra space in the cavity? What exactly is the physiological purpose of their interaction with steroids?

Acknowledgments—We thank P. Deuerling, U. Herzing, and R. Hofmann for expert technical assistance.

REFERENCES

1. Vieths, S. (1997) in *Handbook of Plant and Fungal Toxicants* (D'Mello, J. P. F., ed) pp. 157–174, CRC Press, Boca Raton, FL
2. Kuby, J. (1992) *Immunology*, pp. 359–372, Freeman, New York
3. Breiteneder, H., Pettenburger, K., Bito, A., Valenta, R., Kraft, D., Rumpold, H., Scheiner, O., and Breitenbach, M. (1989) *EMBO J.* **8,** 1935–1938
4. Breiteneder, H., Hoffmann-Sommergruber, K., O'Riordain, G., Susani, M., Ahorn, H., Ebner, C., Kraft, D., and Scheiner, O. (1995) *Eur. J. Biochem.* **233,** 484–489
5. Vanek-Krebitz, M., Hoffmann-Sommergruber, K., Laimer da Camara Machado, M., Susani, M., Ebner, C., Kraft, D., Scheiner, O., and Breiteneder, H. (1995) *Biochem. Biophys. Res. Commun.* **214,** 538–551
6. Scheurer, S., Metzner, K., Haustein, D., and Vieths, S. (1997) *Mol. Immunol.* **34,** 619–629
7. Karamloo, F., Scheurer, S., Wangorsch, A., May, S., Haustein, D., and Vieths, S. (2000) *J. Chromatogr. B Biomed. Appl.*, in press
8. Vieths, S., Karamloo, F., Lüttkopf, D., Scheurer, S., Fötisch, K., May, S., Altmann, F., Skov, P. S., and Haustein, D. (2000) *Arbeiten Paul Ehrlich Inst. Bundesamt Sera Inpfstoffe Frank. A. M.* **93,** 159–168
9. Faber, C., Lindemann, A., Sticht, H., Ejchart, A., Kungl, A., Susani, M., Frank, R. W., Kraft, D., Breitenbach, M., and Rösch, P. (1996) *J. Biol. Chem.* **271,** 19243–19250
10. Gajhede, M., Osmark, P., Poulsen, F. M., Ipsen, H., Larsen, J. N., van Neerven, R. J. J., Schou, C., Løwenstein, H., and Spangfort, M. D. (1996) *Nat. Struct. Biol.* **3,** 1040–1045
11. Schweimer, K., Sticht, H., Nerkamp, J., Boehm, M., Breitenbach, M., Vieths, S., and Rösch, P. (1999) *Appl. Magn. Reson.* **17,** 449–464
12. Holm, J., Henriksen, A., Larsen, J. N., Ipsen, H., Gajhede, M., and Spangfort, M. D. (2000) *Allergy* **55,** Suppl. 63, 21
13. Schöning, B., Vieths, S., Petersen, A., and Baltes, W. (1995) *J. Sci. Food Agric.* **67,** 431–440
14. Hoffmann-Sommergruber, K. (2000) *Int. Arch. Allergy Immunol.* **122,** 155–166
15. Breiteneder, H., and Ebner, C. (2000) *J. Allergy Clin. Immunol.* **106,** 27–36
16. Swoboda, I., Scheiner, O., Heberle-Bors, E., and Vicente, O. (1995) *Plant Cell Environ.* **18,** 865–874
17. Bufe, A., Spangfort, M. D., Kahlert, H., Schlaak, M., and Becker, W.-M. (1996) *Planta* **199,** 413–415
18. Mirza, O., Henriksen, A., Ipsen, H., Larsen, J. N., Wissenbach, M., Spangfort, M. D., and Gajhede, M. (2000) *J. Immunol.* **165,** 331–338
19. Ferreira, F., Ebner, C., Kramer, B., Casari, G., Briza, P., Kungl, A. J., Grimm, R., Jahn-Schmid, B., Breiteneder, H., Kraft, D., Breitenbach, M., Rheinberger, H.-J., and Scheiner, O. (1998) *FASEB J.* **12,** 231–242
20. Scheurer, S., Son, D. Y., Boehm, M., Karamloo, F., Franke, S., Hoffmann, A., Haustein, D., and Vieths, S. (1999) *Mol. Immunol.* **36,** 155–167
21. Valenta, R., Vrtala, S., Focke-Tejkl, M., Bugajska-Schretter, A., Ball, T., Twardosz, A., Spitzauer, S., Grönlund, H., and Kraft, D. (1999) *Biol. Chem.* **380,** 815–824
22. Boehm, M., and Rösch, P. (1997) *Biol. Chem.* **378,** 687–695
23. Neudecker, P., Schweimer, K., Nerkamp, J., Boehm, M., Scheurer, S., Vieths, S., Sticht, H., and Rösch, P. (2000) *J. Biomol. NMR* **8,** 71–72
24. Sluyterman, L. A. Ae., and Elgersma, O. (1978) *J. Chromatogr.* **150,** 17–30
25. Talluri, S., and Wagner, G. (1996) *J. Magn. Reson. B* **112,** 200–205
26. Cavanagh, J., Fairbrother, W. J., Palmer, A. G., and Skelton, N. J. (1996) *Protein NMR Spectroscopy*, pp. 447–453, Academic Press, San Diego
27. Frenkiel, T., Bauer, C., Carr, M. D., Birdsall, B., and Feeney, J. (1990) *J. Magn. Reson.* **90,** 420–425
28. Ikura, M., Bax, A., Clore, G. M., and Gronenborn, A. M. (1990) *J. Am. Chem. Soc.* **112,** 9020–9022
29. Diercks, T., Coles, M., and Kessler, H. (1999) *J. Biomol. NMR* **15,** 177–180
30. Sklenár, V., Piotto, M., Leppik, R., and Saudek, V. (1993) *J. Magn. Reson. A* **102,** 241–245
31. Schleucher, J., Schwendinger, M., Sattler, M., Schmidt, P., Schedletzky, O., Glaser, S. J., Sørensen, O. W., and Griesinger, C. (1994) *J. Biomol. NMR* **4,** 301–306
32. Marion, D., Ikura, M., Tschudin, R., and Bax, A. (1989) *J. Magn. Reson.* **85,** 393–399
33. Dayie, K. T., and Wagner, G. (1994) *J. Magn. Reson. A* **111,** 121–126
34. Johnson, B. A., and Blevins, R. A. (1994) *J. Biomol. NMR* **4,** 603–614
35. Brünger, A. T. (1992) *X-PLOR Version 3.1*: A *System for X-ray Crystallography and NMR*, The Howard Hughes Medical Institute and Department of Molecular Biophysics and Biochemistry, Yale University, New Haven, CT
36. Nilges, M., Clore, G. M., and Gronenborn, A. M. (1988) *FEBS Lett.* **229,** 317–324
37. Nilges, M., Clore, G. M., and Gronenborn, A. M. (1988) *FEBS Lett.* **239,** 129–136
38. Nilges, M., Gronenborn, A. M., Brünger, A. T., and Clore, G. M. (1988) *Protein Eng.* **2,** 27–38
39. Holak, T. A., Nilges, M., and Oschkinat, H. (1989) *FEBS Lett.* **242,** 218–224
40. Beiβinger, M., Sticht, H., Sutter, M., Ejchart, A., Haehnel, W., and Rösch, P. (1998) *EMBO J.* **17,** 27–36
41. Sticht, H., Pickford, A. R., Potts, J. R., and Campbell, I. D. (1998) *J. Mol. Biol.* **276,** 177–187
42. Kuszewski, J., Gronenborn, A. M., and Clore, G. M. (1996) *Protein Sci.* **5,** 1067–1080
43. Powell, M. J. D. (1977) *Math. Progr.* **12,** 241–254
44. Laskowski, R. A., MacArthur, M. W., Moss, D. S., and Thornton, J. M. (1993) *J. Appl. Crystallogr.* **26,** 283–291
45. Brünger, A. T., Clore, G. M., Gronenborn, A. M., Saffrich, R., and Nilges, M. (1993) *Science* **261,** 328–331
46. Laemmli, U. K. (1970) *Nature* **227,** 680–685
47. Vieths, S., Schöning, B., and Baltes, W. (1992) *Food Agric. Immun.* **4,** 181–197
48. Laskowski, R. A. (1995) *J. Mol. Graphics* **13,** 323–330
49. Kleywegt, G. J., and Jones, T. A. (1998) *Acta Crystallogr. Sect. D Biol. Crystallogr.* **54,** 1119–1131
50. Ghosh, D., Wawrzak, Z., Pletnev, V. Z., Li, N., Kaiser, R., Pangborn, W., Jörnvall, H., Erman, M., and Duax, W. L. (1995) *Structure* **3,** 279–288
51. Kuszewski, J., and Clore, G. M. (2000) *J. Magn. Reson.* **146,** 249–254
52. Tsujishita, Y., and Hurley, J. H. (2000) *Nat. Struct. Biol.* **7,** 408–414
53. Holm, L., and Sander, C. (1993) *J. Mol. Biol.* **233,** 123–138
54. Fujioka, S. (1999) in *Brassinosteroids* (Sakurai, A., Yokota, T., and Clouse, S. D., eds) pp. 21–45, Springer, Tokyo
55. Guex, N., and Peitsch, M. C. (1997) *Electrophoresis* **18,** 2714–2723
56. Barton, G. J. (1993) *Protein Eng.* **6,** 37–40
57. Kraulis, P. J. (1991) *J. Appl. Crystallogr.* **24,** 946–950
58. Merritt, E. A., and Murphy, M. E. P. (1994) *Acta Crystallogr. Sect. D Biol. Crystallogr.* **50,** 869–873